Parameterization of urban sensible heat flux from remotely sensed surface temperature Effects of surface structure

Yang, Jinxin; Menenti, Massimo; Krayenhoff, E. Scott; Wu, Zhifeng; Shi, Qian; Ouyang, Xiaoying

DOI
10.3390/rs11111347

Publication date
2019

Document Version
Final published version

Published in
Remote Sensing

remote sensing

MDPI

Article

Parameterization of Urban Sensible Heat Flux from Remotely Sensed Surface Temperature: Effects of Surface Structure

Jinxin Yang [1], Massimo Menenti [2,3], E. Scott Krayenhoff [4], Zhifeng Wu [1,*], Qian Shi [5] and Xiaoying Ouyang [3]

1 School of Geographical Sciences, Guangzhou University, Guangzhou 510006, China; yangjx11@gzhu.edu.cn
2 Faculty of Civil Engineering and Earth Sciences, Delft University of Technology, P.O. Box 5048, 2600 GA Delft, The Netherlands; m.menenti@tudelft.nl
3 State Key Laboratory of Remote Sensing Science, Institute of Remote Sensing and Digital Earth, Chinese Academy of Sciences, Beijing 100101, China; ouyangxy@radi.ac.cn
4 School of Environmental Sciences, University of Guelph, 50 Stone Road East, Guelph, ON N1G 2W1, Canada; skrayenh@uoguelph.ca
5 School of Geography and Planning, Sun Yat-sen University, Guangzhou 510275, China; shixi5@mail.sysu.edu.cn
* Correspondence: zfwu@gzhu.edu.cn; Tel.: +86-132-2642-4942

Received: 23 April 2019; Accepted: 24 May 2019; Published: 4 June 2019

Abstract: Sensible heat exchange has important consequences for urban meteorology and related applications. Directional radiometric surface temperatures of urban canopies observed by remote sensing platforms have the potential to inform estimations of urban sensible heat flux. An imaging radiometer viewing the surface from nadir cannot capture the complete urban surface temperature, which is defined as the mean surface temperature over all urban facets in three dimensions, which includes building wall surface temperatures and requires an estimation of urban sensible heat flux. In this study, a numerical microclimate model, Temperatures of Urban Facets in 3-D (TUF-3D), was used to model sensible heat flux as well as radiometric and complete surface temperatures. Model data were applied to parameterize an effective resistance for the calculation of urban sensible heat flux from the radiometric (nadir view) surface temperature. The results showed that sensible heat flux was overestimated during daytime when the radiometric surface temperature was used without the effective resistance that accounts for the impact of wall surface temperature on heat flux. Parameterization of this additional resistance enabled reasonably accurate estimates of urban sensible heat flux from the radiometric surface temperature.

Keywords: sensible heat flux; radiometric temperature; complete urban surface temperature; urban geometry

1. Introduction

Urban surface energy balance strongly modulates fair weather urban climates [1]. The replacement of soil or vegetation by impervious surfaces in urban areas reduces the potential for mitigation of ambient temperature through evaporation and transpiration [2–4]. Instead, the absorbed radiative energy is largely dissipated as sensible heat flux, warming the atmosphere. Turbulent heat exchange in urban areas is a major component of heat and mass transfer from the urban canopy to the atmospheric boundary layer, and sensible heat flux is a major component of turbulent exchange. Generally, turbulent heat exchange in urban areas can be modeled by microclimate or computational fluid dynamics [5] numerical simulation models [6–10] or estimated by the bulk transfer approach [11–13].

Detailed modeling of turbulent heat and mass transport in urban areas is computationally very demanding [6,14–16]. The bulk heat transfer approach assumes the surface to be homogeneous and horizontal, with sensible heat flux being proportional to the surface–air temperature difference divided by aerodynamic resistance [17].

The complex geometry of urban areas presents a challenge in the estimation of sensible heat flux [18]. One reason is that the geometric characteristics of urban areas change aerodynamic resistance, depending on both shape and spatial arrangement [18]. The air–surface interface must be taken into account to parameterize land–atmosphere heat and mass exchanges. This is especially important for resistance parameterization in urban areas, since urban surface temperature is heterogeneous because of urban structures [5,19]. When we use the bulk transfer method to estimate sensible heat flux, it should be noted that such a resistance-based parameterization of sensible heat flux is 1D, i.e., it defines a horizontal, homogeneous surface and its temperature in such a way that the sensible heat flux density is the same as the one applied to the actual 3D urban surface.

Urban energy exchange studies using remotely sensed data are increasingly common because remote sensing is an important ground observation method and can provide information that is spatially extensive, continuous, and detailed [20–29]. The estimation of sensible heat flux with remote sensing data is based on the bulk transfer approach, which relies on observations of the temperature gradient [17,22,30]: Thus an appropriate parameterization should be developed. The radiometric surface temperature observed by remote sensing depends on the specific area of building facets due to shading by buildings and is not the complete surface temperature of targets. The complete surface temperature is the area-weighted mean temperature of all component facets under heterogeneous thermal conditions, which is needed to estimate urban sensible heat flux [31]. There is heat exchange between all component facets and the air within the urban canopy and between the urban canopy and the atmospheric boundary layer. Thus, the complete surface temperature is needed. As remote sensors tend to be limited in their capability to observe all facets in urban areas, it is a challenge to retrieve the urban complete surface temperature of heterogeneous mixed pixels from remote sensing data [32–34]. The complete surface temperature is required to calculate sensible heat flux [31], however, since a biased surface temperature causes a bias in sensible heat flux estimates [11]. Reference [11] evaluated the use of different temperatures to estimate sensible heat flux from airborne and ground measurements and concluded that the temperature should be chosen carefully, since different temperatures can cause large biases. Aerodynamic resistance is defined by an equation relating sensible heat flux to the temperature difference between the surface and atmosphere at reference height [17]. Thus, different resistance parameterizations should be considered for different temperatures. Kanda et al. [13] analyzed the impact of using the radiometric surface temperature instead of the complete surface temperature to estimate sensible heat flux, and the results showed that this impact should be corrected by improving the resistance estimation.

In order to estimate sensible heat flux accurately from observed radiometric surface temperatures through field measurements or remote sensing, the impact of the difference between the radiometric and complete surface temperature should be parameterized. Troufleau et al. [35] investigated the use of radiometric temperature to estimate sensible heat flux over sparse vegetation and showed that there is an important difference between the radiometric surface temperature observed over a vegetation canopy and the foliage temperature within it: They then explored a parameterization of the aerodynamic resistance to reduce the bias from sensible heat flux caused by using the radiometric surface temperature to estimate sensible heat flux. Since the radiometric surface temperature observed over a vegetation canopy is different from the actual foliage temperature due to light interception by leaves, Zhao et al. [36] evaluated the use of the leaf area index (LAI) in parameterizing the extra resistance to heat transfer when the radiometric surface temperature is used to estimate the sensible heat flux. This means adding extra resistance is a good choice to correct for bias due to the difference between radiometric and real surface temperature.

Although more and more studies have used radiometric surface temperature to estimate the sensible heat flux in urban areas [3,22,37,38], the effects of directly using the radiometric surface temperature instead of the real surface temperature in the estimation of urban sensible heat flux have received scant attention. Thus, this study explores how the resistance changes when different temperatures are used to estimate sensible heat flux and how to parameterize the extra resistance when the radiometric surface temperature is used for sensible heat flux estimation.

The primary method for estimating resistance is based on measured sensible heat flux and the air–surface temperature difference [17]. Based on a number of observations or simulations, relationships between aerodynamic resistance and geometric parameters combined with local climate variables can be evaluated, and then aerodynamic resistance can be parameterized using geometric parameters and local climate variables [39]. This provides a possible way to estimate resistance and then estimate sensible heat flux based on the observed surface and air temperature. Since the complete surface temperature and radiometric surface temperature may be very different [32], the aerodynamic resistance applicable to estimates of sensible heat flux from the radiometric temperature or complete surface temperature can strongly differ. This means that different aerodynamic resistances should be used for estimating sensible heat flux, depending on the surface temperature used. Widely used parameterizations of aerodynamic resistance apply to the estimation of urban sensible heat flux using the complete surface temperature [11–13]. When radiometric surface temperature is used, an appropriate parameterization of the aerodynamic resistance should be applied.

Thus, this study explores the consequences of using different temperatures, i.e., the radiometric versus the complete urban surface temperature, on the resistance of sensible heat flux estimations. Specifically, we determined the aerodynamic resistance in each case to estimate sensible heat flux under different geometric and meteorological conditions using data generated by numerical experiments with an urban climate model named Temperatures of Urban Facets in 3-D (TUF-3D), which is a microscale urban energy balance model [40]. A parameterization of resistances for estimating the sensible heat flux in urban areas using observations of the urban radiometric surface temperature was developed, since this temperature is easily retrieved with imaging radiometers.

The objective of this study was to derive an effective resistance for the calculation of urban sensible heat flux from radiometric (nadir view) surface temperature. Modeled data generated through numerical experiments with the TUF-3D model were used for this purpose.

The methodology of combining different temperatures with appropriate resistances to estimate sensible heat flux in an urban environment is introduced in Section 2. The results of different resistance parameterizations and sensible heat fluxes are in Section 3. A discussion and conclusions are in Sections 4 and 5, respectively.

2. Methodology and Data

2.1. TUF-3D

A version of the TUF-3D microscale urban energy balance model [40] that is optimized for regular building arrays was applied to independently model the sensible heat flux of multiple combinations of geometric parameters and local meteorological conditions [40]. Facet temperature is calculated based on the facet energy balance. TUF-3D fluxes and (sub)facet surface temperatures have been evaluated against measurements from two midlatitude cities [39], and the model was subsequently applied to evaluate radiation models [41] and to provide surface temperatures for remote sensing research [42]. For sensible heat flux estimation, the profiles of wind speed and air temperature are a function of urban morphology and above-canyon forcing, and they drive sensible heat exchange from patches at each height. TUF-3D has also been used to simulate the sensible heat fluxes in a lightweight low-rise neighborhood in Andacollo, Chile, and the results were compared to observations and a local-scale empirical model (LUMPS) for a 14-day period in the autumn of 2009. The results showed good agreement between observed and modeled sensible heat fluxes [43]. TUF-3D was originally

tested against urban climate, surface temperature, and energy balance data from Vancouver, Canada, and Basel, Switzerland, and it has been applied in diverse cities. These prior model evaluations support the application of TUF-3D in modeling urban sensible heat flux, the complete and radiometric surface temperatures for different urban geometries and seasons. More details about facet surface temperature and sensible heat flux simulation in TUF-3D can be found in [39].

2.2. Complete versus Radiometric Urban Surface Temperature

Urban complete surface temperature (T_c) was defined by Voogt and Oke [31] as the area-weighted temperature of total component areas, and it can be calculated from the facet temperatures provided by TUF-3D. In this study, we define T_r as the radiometric temperature observed by remote sensing from a nadir-view angle. In Reference [44], radiometric temperature was defined as the temperature calculated from the area-weighted average of emittance by the observed surfaces after emissivity correction and atmospheric correction. In this study, T_r was calculated from the upwelling radiation from roofs and roads, since the narrow fields of view of satellite sensors limited observations of wall facets by nadir-viewing imaging radiometers. The upwelling radiation of roofs and roads includes the radiation emitted by roofs and the ground (e.g., road) and the longwave radiation reflected by roads and roofs originally emitted by building walls and by the atmosphere. The reflected part of radiation depends on the wall surface temperature and material emissivity of walls and roads, as well as sensor-ground geometry. For radiometric temperature retrieval, the upwelling radiance (exitance) at the bottom of the atmosphere is written as

$$L_r = \varepsilon \sigma T_r^4 + (1 - \varepsilon) L_d, \tag{1}$$

where ε is the emissivity of the surface observed by an imaging radiometer. In this study, the emissivity of walls, roads, and roofs was set as 0.9, 0.95, and 0.91, respectively, according to Reference [45]. Here, ε is calculated as the area-weighted average of road and roof emissivity. L_d is the downwelling atmospheric radiation at the surface, and T_r is the radiometric temperature measured by a nadir-view imaging radiometer. TUF-3D provides the upwelling radiation from roads and roofs, including reflected radiation. Then, L_r can be calculated as the area-weighted average of radiation from roofs and roads. L_d is calculated from an atmospheric profile in TUF-3D.

2.3. Parameterization of Sensible Heat Flux

The sensible heat exchange between the urban surface and the atmosphere boundary layer can be written as [11,12]

$$Hs = \rho C_p \frac{(T_c - T_a)}{r_h}, \tag{2}$$

where r_h (s/m) is the resistance to heat transfer when the complete surface temperature T_c is used to replace the aerodynamic near-surface air temperature. T_a is the air temperature at the reference height, which is set at twice the building height in TUF-3D. C_p is the specific heat of air at a constant pressure (J kg^{-1} K^{-1}), i.e., 1003.5 J kg^{-1} K^{-1} at 20 °C, and ρ is air density (kg m^{-3}), calculated from air pressure, air temperature, and humidity.

When the radiometric surface temperature is used to estimate sensible heat flux, another resistance is added to Equation (2) to reduce the bias caused by the difference between complete surface temperature (T_c) and radiometric surface temperature (T_r) (1):

$$Hs = \rho C_p \frac{(T_r - T_a)}{r_h + r_r}. \tag{3}$$

T_r is the radiometric surface temperature observed by remote sensing at nadir, and r_r is extra resistance to correct for the difference between urban radiometric and complete surface temperature.

2.4. Parameterization of Resistance to Heat Transfer

Parameterization of the resistance for different urban temperatures has not been studied, and different kinds of surface temperatures are frequently unavailable. Thus, this study analyzed the impact of different surface temperatures on resistance to sensible heat flux transfers and parameterized the extra resistance applicable when the directional (nadir) radiometric temperature was used to estimate sensible heat flux. According to Equation (2), when the sensible heat flux and complete surface temperatures are known, the resistances can be calculated as

$$r_h = \rho C_p \frac{(T_c - T_a)}{Hs}. \quad (4)$$

According to Equation (3), when the radiometric temperature is used, the total resistance can be written as

$$r_h + r_r = \rho C_p \frac{(T_r - T_a)}{Hs}. \quad (5)$$

According to Equations (4) and (5), r_r can be written as

$$r_r = \rho C_p \frac{(T_r - T_c)}{Hs}, \quad (6)$$

where r_h and r_r were determined using the sensible heat flux and temperatures provided by TUF-3D. Here, r_r is directly related to the remotely sensed radiometric temperature and applies to the difference between T_r and T_c (Equation (6)).

In urban areas, the differences between T_r and T_c are affected by urban geometry (planar area index λ_p and the aspect ratio) and local meteorological conditions (solar radiation and wind, principally, for clear sky conditions), since these factors affect the surface energy exchange and the temperature distribution. Here, we added a diurnal plot of T_c and T_r for four dates (different seasons) when λ_p is 0.25 and the ratio of building height to length (*H/L*) is 1.0 (Figure A1 in the Appendix A). In this condition, the difference between T_c and T_r can reach 8 °C at noon in the summer and 5 °C at noon in the winter. When λ_p and *H/L* increase, the difference between T_c and T_r increases. The planar area index λ_p is calculated as the ratio of a building's area to the area of a building's footprint [39]. The differences between T_r and T_c are caused by the wall surface temperature distribution. The surface energy exchange of walls is affected by λ_p, the aspect ratio, and material properties, since these factors determine the radiative and convective heat transfer from a wall to the atmosphere boundary layer. Urban surface material properties can exhibit large and complicated spatial variability. Here, we focused on the effects of geometric parameters and local climate variables, i.e., λ_p, the aspect ratio, solar irradiance, and wind, on different resistances and on the parameterization of the different resistances. The wall facet area index (*F*), calculated as the ratio of the wall area of a building to the area of a building's footprint, is related to building density and the aspect ratio. Thus, *F* and λ_p will be applied to characterize building geometry in this study. Table 1 showed the definitions of the different temperatures, resistances, and geometric parameters used in this study.

Table 1. Definitions of the different temperatures, resistances, and geometric parameters used in this study.

Parameters	
T_c	complete surface temperature
T_r	radiometric surface temperature observed by remote sensing at a nadir angle
r_h	r_h (s/m) is the resistance to heat transfer when the complete surface temperature T_c is used to replace the aerodynamic near-surface air temperature
r_r	the extra resistance to correct for the difference between urban radiometric and complete surface temperature
λ_p	the ratio of a building's area to the area of a building's footprint
F	the ratio of the wall area of a building to the area of a building's footprint
H/L	the ratio of building height to length

2.5. Experimental Design

In order to explore how to parameterize the resistances used to estimate sensible heat flux, TUF-3D was applied to model the sensible heat flux, radiometric surface temperature, and complete surface temperature for different solar angles and urban geometries, e.g., different λ_p and aspect ratios (Table 2). The aspect ratio is defined as the ratio of a building's height to street width, and it can be determined by λ_p and the ratio of a building's height to a building's width (H/L). In the version of TUF-3D applied here, all buildings have square footprints. Here, λ_p and H/L are modulated, which changes both the building density and aspect ratio in TUF-3D. Note that the ratio of a building's height to the street width changes with both λ_p and H/L. TUF-3D performs better during daytime, and thus results from the daytime (8:00 to 17:00) will be analyzed [43].

Table 2. Numerical experiments with Temperatures of Urban Facets in 3-D (TUF-3D): geometric conditions and input data.

Geometric Range	Dates for Analysis	Dates for Evaluation	Variables
λ_p: 0.05~0.60 H/L: 0.5 to 6	12 Apr. 2010 (case 1) 29 Aug. 2010 (case 2) 28 Oct. 2010 (case 3) 18 Dec. 2010 (case 4)	27 Feb. 2010 1 Jul. 2010 17 Sept. 2010 27 Nov. 2010	solar radiation wind speed air temperature air pressure at ground surface

We varied the λ_p value from 0.05 to 0.6 with 0.05 steps and the ratio of building height to width (H/L) from 0.5 to 6 with 0.5 steps in our numerical experiments with TUF-3D, which thus explored most urban densities and aspect ratios [45]. The λ_p and H/L determine the aspect ratio in TUF-3D. Meteorological data, i.e., solar radiation, wind speed, air temperature, and air pressure, on eight sunlit days were collected from a weather station at the Hong Kong Observatory to model sensible heat flux and the radiometric and complete surface temperatures: 27 February 2010 and 12 April 2010 (spring); 1 July 2010 and 29 August 2010 (summer); 17 September 2010 and 28 October 2010 (autumn); 27 November 2010 and 18 December 2010 (winter). Resistances were then computed using either radiometric or complete surface temperature. In this study, the latitude was set as 22.15° N. An overview of the numerical experiments is given in Table 1. The data from 0:00 to 24:00 were simulated, but only the data from 8:00 to 17:00 were used in this study.

The sensible heat flux, complete surface temperature, and radiometric temperature were modeled under different forcing and geometric conditions. The simulated data on four days were used to determine the resistances according to Equations (4)–(6). Solar angles affected the sunlit and shaded facet distribution and then affected the surface energy heat exchange. Solar angles were calculated from the latitude and day of the year as well as the time of day. In order to study the impact of solar angles on the different resistances, different days of the year were included in the numerical experiments (i.e., 1, 45, 90, 135, 180, 225, 270, 315) based on the same meteorological variables. Next, the dependence of r_h and r_r on geometric parameters and local climate variables was analyzed and parameterized. Finally, parameterizations of r_h and r_r were developed and evaluated against independently simulated days in terms of sensible heat flux predictions.

2.6. Evaluation of the Parameterizations

Thermal images with 0.5 m of spatial resolution observed by an airborne thermal camera at noontime (12:40 to 13:00) on 6 August 2013 in urban areas of the Kowloon Peninsula (Figure 1) were used to evaluate the parameterization of r_r. The FOV (Field angle of view) of the thermal camera was 24° and the flight height was 500 m. The complete urban surface temperature (T_c) was estimated from high-resolution thermal data and GIS building data. The building GIS data could provide λ_p and F in this study. More information about the high-resolution thermal images and building data is referred to in Reference [33]. The radiometric temperature (T_r) was obtained by aggregating to a lower spatial resolution the high-resolution thermal images observed from a nadir or near-nadir direction. Then T_c

was used to estimate the sensible heat flux in Equation (2), and r_h in Equation (2) could be estimated as it was in Voogt and Grimmond (2001) and Yang et al. (2016). T_r was used to estimate the sensible heat flux in Equation (3), and r_r was calculated from urban building data and meteorological data from the Hong Kong Observatory using the parameterizations developed in this study. Then the sensible heat fluxes from Equations (2) and (3) were compared. If both parameterizations were correct, the values of sensible heat fluxes given by Equation (2) should have been the same as the values of sensible heat fluxes given by Equation (3). Figure 2 is a flow chart of this study.

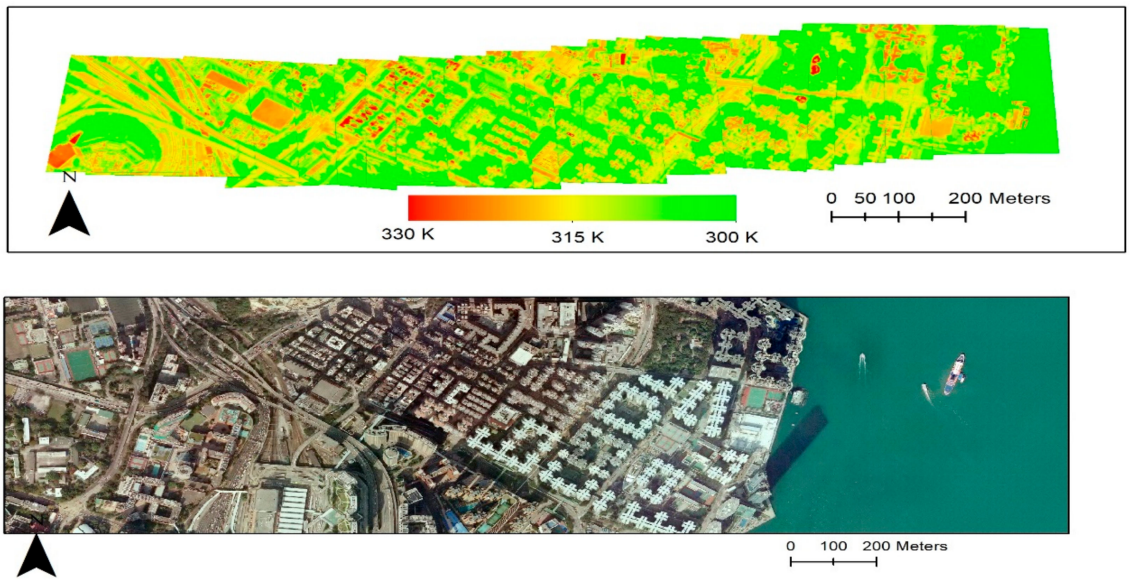

Figure 1. High-resolution thermal images.

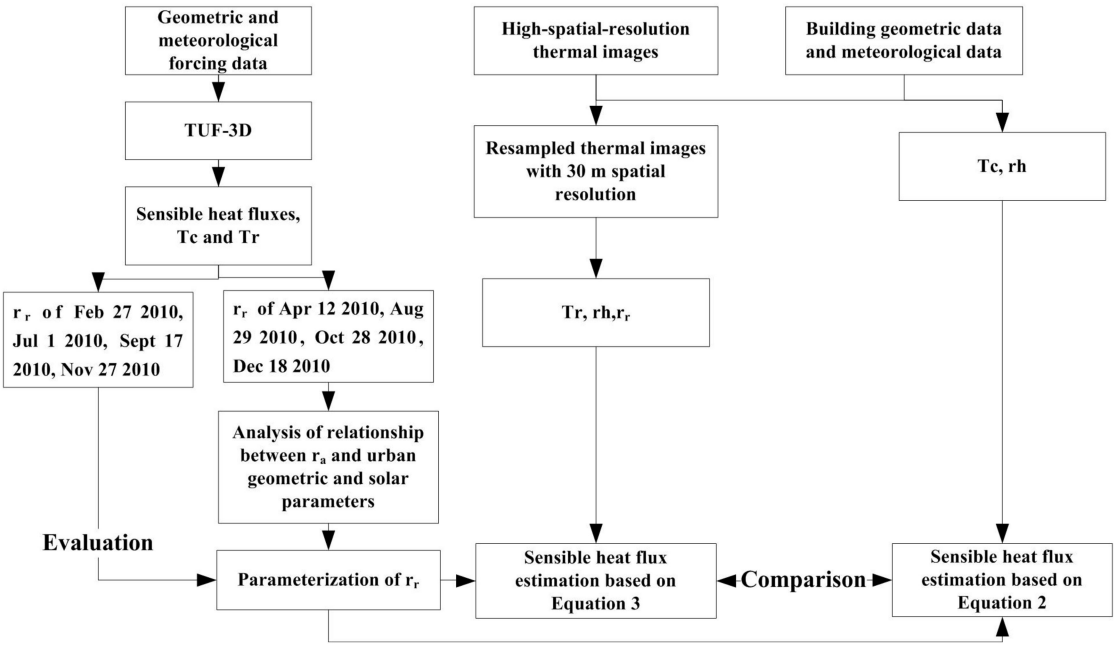

Figure 2. Flow chart of this study.

3. Results

3.1. Sensitivity of r_h and r_r to Urban Geometry and Meteorological Forcing

Here, r_h, $r_h + r_r$, and r_r were calculated with Equations (5) and (6) using the data generated with the TUF-3D numerical experiments when λ_p varied from 0.05 to 0.60 and H/L from 0.5 to 6. Figure 3

illustrates the dependence of r_h, $r_h + r_r$, and r_r on λ_p for buildings with a moderate vertical extent when different surface temperatures were used. Here, we only show two kinds of *H/L* values (*H/L* = 2 and *H/L* = 3) as an example to explain the change of resistances with λ_p. As λ_p increased, r_h decreased, because T_c decreased more rapidly than sensible heat flux as the fraction of the 3D surface area that was shaded grew (Appendix A Figure A2a,b).The sensible heat flux decreased with λ_p first, since the buildings became closer together and roughness could decrease. Skimming flow appeared, and the overall surface roughness could decrease [39], and thus the sensible heat flux decreased first. With the increase of λ_p, the displacement length also increased. This could cause a slight increase of sensible heat flux when λ_p was larger than 0.44 in some cases (Appendix A Figure A1).

When the nadir radiometric surface temperature (T_r) was used to estimate sensible heat flux (Equation (2)), the relation between λ_p and resistance ($r_h + r_r$) (Figure 3) was different than when T_c was used for the same sensible heat flux values (Figure 3). The change of T_r with λ_p was not monotonic (Appendix A Figure A2c), and thus the trends of resistance $r_h + r_r$ as a function of λ_p changed with the season. As seen in Figure 3a,b, $r_h + r_r$ increased when λ_p increased, while (in Figure 3c) $r_h + r_r$ even decreased when λ_p increased. As seen in Figure 3d, $r_h + r_r$ decreased, then increased when λ_p increased. The extra resistance r_r for radiometric surface temperature kept increasing with λ_p (Figure 3) because the difference between T_c and T_r increased with λ_p. Additionally, r_r could be several times higher than r_h. This means that extra resistance r_r should be added to estimate sensible heat flux correctly when the radiometric surface temperature is used. In addition, the relation between r_r and λ_p was in good agreement with the linear relationship under different conditions (Appendix A, Table A1). The correlation coefficients between r_r and λ_p were higher than 0.92 in the simulations of cases 1–4 (Appendix A, Table A1: 12 April 2010 (case 1), 29 August 2010 (case 2), 28 October 2010 (case 3), 18 December 2010 (case 4)) under different meteorological and structural conditions. This made it possible to parameterize r_r. Thus, adding r_r to estimate sensible heat flux using the radiometric surface temperature was feasible.

The change of T_r with λ_p was affected by solar angles (Appendix A Figure A2c,d), and this also made the related resistances change. On 29 August 2010, the solar zenith angle was lower than on the other days, and thus the effects of added shadow caused by increasing λ_p were smaller than the increase in the fractional area of rooftops, and T_r increased with the increase in λ_p. The area of wall facets per unit of horizontal area increased with increasing λ_p. This increased the fraction of urban area that was not captured by a nadir-looking radiometer, thus increasing the difference between T_r and T_c, leading to a higher r_r at higher λ_p. On other days, the solar zenith angle was higher, and thus the shadow areas increased when λ_p increased. This made T_r decrease with λ_p first (Appendix A Figure A2c,d). When λ_p kept increasing, the shadow areas on a horizontal surface did not increase because of dense high-rise buildings. This made T_r start to increase with λ_p. This was very obvious on 17 December 2010, since wind speed was lower than on other days. The trend in $r_h + r_r$ on 17 December 2010 was similar to the trend in T_r with respect to λ_p.

The resistances were affected by wind speed and solar radiation. Solar radiation on 29 August 2010 was higher than on other days, and thus r_r was higher than on other days and increased more rapidly with λ_p. The resistances on 18 December 2010 were larger than on 28 October 2010, since wind speed on 18 December 2010 was 1.1 m/s, while it was 3.9 m/s on 28 October 2010. Wind speed not only affected aerodynamic resistance, but also affected r_r, since it affected the energy exchange at a wall surface and thus the difference between T_c and T_r.

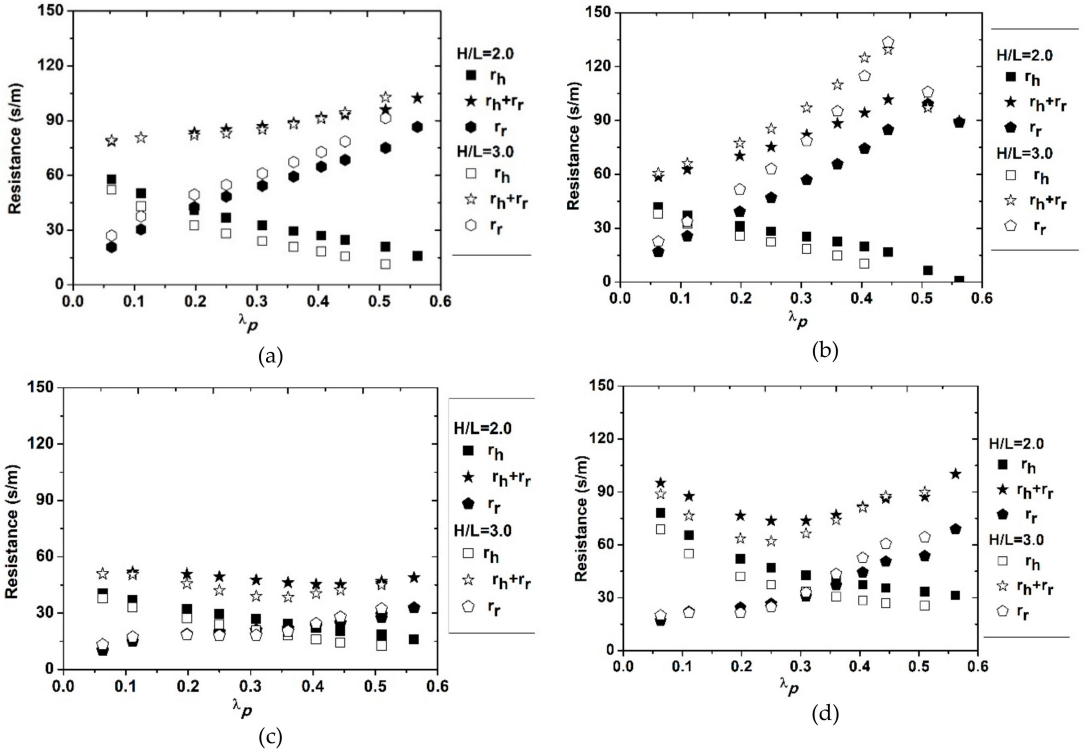

Figure 3. Resistances (r_h, $r_h + r_a$, r_a, $r_h + r_r$, r_r in Equations (2)–(4)) as a function of λ_p for different seasonal conditions: (**a**) 11 April 2010; (**b**) 29 August 2010; (**c**) 28 October 2010; (**d**) 17 December 2010. *H/L* is the building height to width ratio. All buildings had square footprints.

The relationships between resistance and the wall-to-plan area ratio F when different temperatures were used under different conditions are shown in Figure 4. Generally, r_h decreased with increasing F when T_c was used (Figure 4a–d). When F increased, the wall facet areas exposed to solar heating and wind convection increased, and thus it was easier to dissipate the excess heat at a wall through convection with a certain building density. When radiometric surface temperature was used, the trends of $r_h + r_r$ with F were not monotonic, but they were similar to the trend of $r_h + r_r$ versus λ_p. The change of r_r with F was complicated. When r_r was higher than 20 s/m, the relation between r_r and F was logarithmic (Figure 4a,b,d; and Appendix A, Table A2). When r_r was smaller than 20 s/m, the relation between r_r and F was logarithmic only when the aspect ratio was smaller than 3 (Appendix A, Table A2). When λ_p was 0.25 and F was 2, the aspect ratio was 2. When λ_p was larger than 0.1, the aspect ratio was larger than F in TUF-3D. According to Reference [45], the mean aspect ratio in a typical compact high-rise area is about 2.5. Thus, the logarithmic relationship between F and r_r applies to urban areas.

Solar irradiance enhanced the difference between the radiometric and complete surface temperature. The relationship between resistances and F in Figure 4 was also affected by wind speed, as was the relationship between resistances and λ_p (Figure 4). When the wind speed was higher, r_h and $r_h + r_r$ became smaller, as did r_r (Figure 4c,d). As seen in Appendix A, Table A2, the correlation coefficients between r_r and F were higher than 0.85, except for cases when r_r was smaller than 20 s/m.

The solar irradiance of urban facets changes with the solar angle, modifying shadow patterns and facet irradiance [46]. The surface temperatures of the ground, roofs, and walls can undergo very different diurnal cycles because of differences in solar illumination, facet orientation, and material properties [5]. Figure 5 shows the changes in resistance with different solar zenith angles and solar azimuth angles and solar radiation. The results show that r_r increased with decreasing solar zenith angles first and then reached a peak when the solar zenith angle was smallest (highest solar elevation angle). Here, r_h did not obviously change with the different solar zenith angle except on day 360 and

day 315: r_h slightly increased with decreases in the solar zenith angle first, and then decreased with increases in the solar zenith angle. This was similar to r_r. On days 90, 180, and 225, r_h remained almost constant. This meant r_h could be parameterized as a function of surface structure parameters and wind speed in most conditions, as was shown in References [11,39]. Changes in r_r with the solar zenith angle were clear. When the solar zenith angle was small, r_r was highest (Figure 5). The solar azimuth angle also affected shadow distributions and then the differences between the temperatures used in this study. Resistance r_h had no obvious relationship with solar radiation and the solar angle.

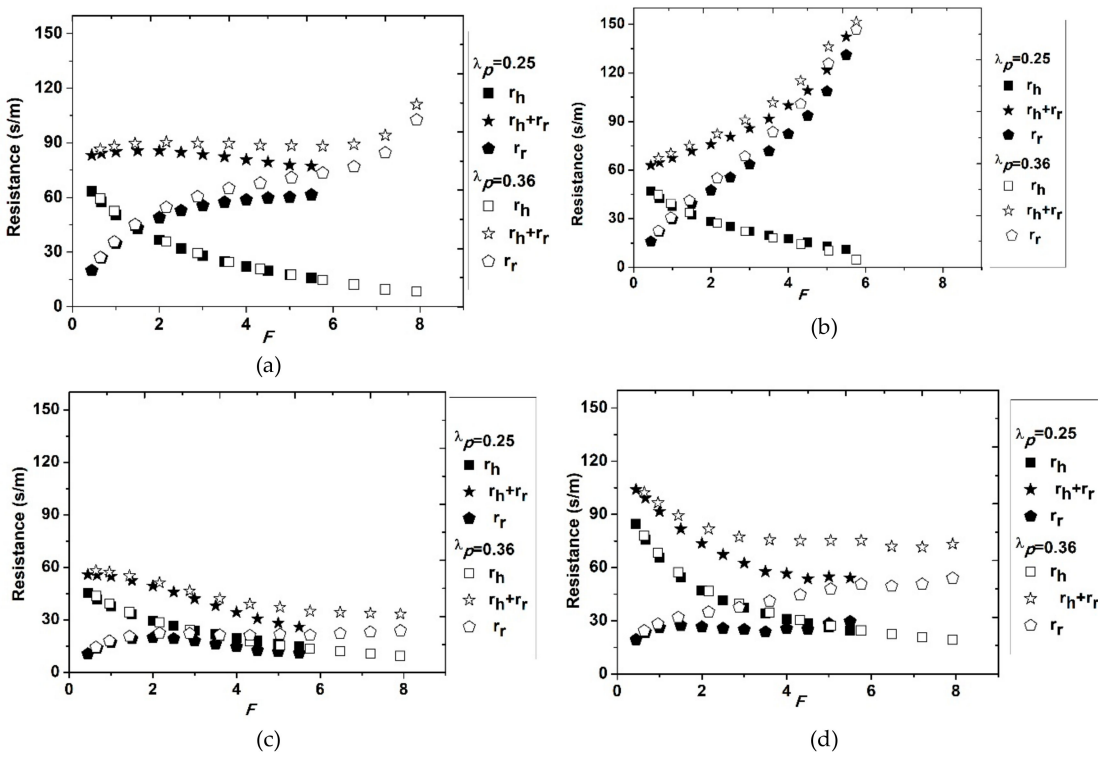

Figure 4. Resistances (r_h, $r_h + r_a$, r_a, $r_h + r_r$, r_r in Equations (2)–(4)) versus F under different conditions: (**a**) 11 April 2010; (**b**) 29 August 2010; (**c**) 28 October 2010; (**d**) 18 December 2010.

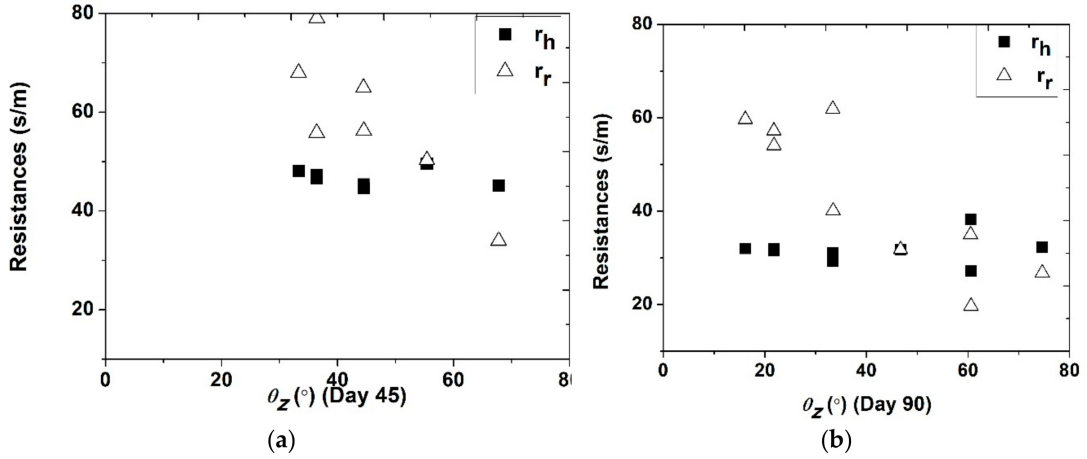

Figure 5. *Cont.*

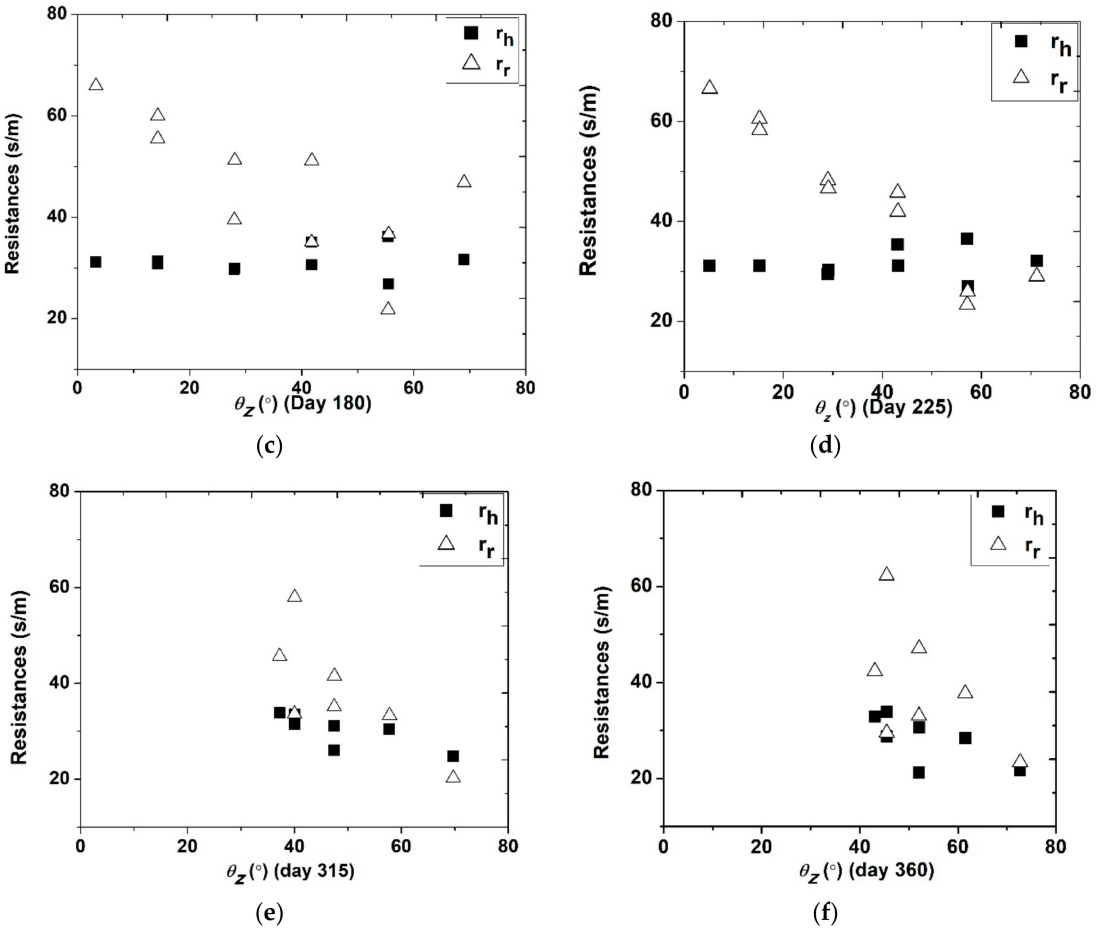

Figure 5. Resistances versus θ_z on different days of the year (DoYs): (**a**) 45; (**b**) 90; (**c**) 180; (**d**) 225; (**e**) 270; and (**f**) 360.

3.2. Parameterization of r_r

Generally, the resistances applicable to T_r are higher than the resistance applicable to T_c in the daytime, and thus if we just used T_r from nadir remote sensing data to replace T_c, the sensible heat flux would be overestimated in daytime. Especially when wind speed is small (<2 m/s), the resistance of T_r can reach more than five times the resistance of T_c: This can cause a large overestimation of sensible heat flux in urban areas if the correct resistance is not used. Considering the current parameterization methods for aerodynamic resistance are based on the T_c used for sensible heat flux estimation, the extra resistance r_r should be added to calculate the sensible heat flux correctly when using the radiometric surface temperature.

As seen in Figures 3 and 4, the trends of $(r_h + r_r)$ with λ_p and F were not monotonic. The additional resistance r_r correlated better with geometric parameters and local climate variables than aerodynamic resistance $(r_h + r_r)$ of radiometric temperature (Figures 3 and 4). This meant that the parameterization of r_r was easier and better than directly parameterizing the aerodynamic resistance of radiometric temperature.

Urban geometry and solar irradiance affected the relation between T_c and T_r as observed by remote sensing. Thus, r_r could be parameterized as a function of urban geometric parameters and solar irradiance. Wind speed at reference height affected aerodynamic resistance, while the extra resistance was caused by the difference between T_r and T_c. The resistances on 18 December 2010 were larger than on 28 October 2010, since the wind speed on 18 December 2010 was 1.1 m/s, while the wind speed was 3.9 m/s on 28 October 2010 (Figures 3 and 4). The wind speed at reference height above the urban canopy could reduce thermal heterogeneity and then reduce the difference between T_r and T_c, and thus

the extra resistance decreased with increasing wind speed. This means that wind speed (w) should be included to parameterize the extra resistance. Thus, a generic empirical parameterization of r_r can be written as

$$r_r = a_1 \ln(F) + a_2 * \lambda_p + a_3 * \theta_a + a_4 * \theta_z + a_5 * Kd + a_6 * w + a_7, \quad (7)$$

where w is wind speed (m s^{-1}), Kd is solar irradiance on a flat surface (W m^{-2}), θ_a is the azimuth angle (°), and θ_z is the zenith angle (°).

The form of the parameterization (Equation (7)) was based on an analysis of the dependence of the additional resistance on geometric parameters. The dependence of r_r on F was logarithmic (Figure 5), while it was nearly linear with λ_p (Figure 4). Similar evaluations (not shown) for the remaining parameters in Equation (7) did suggest a linear relationship. This led us to choose the polynomial form of Equation (7).

The correlation coefficients between r_r and urban geometric parameters and local climate parameters were estimated using the simulated data (Table 3). When the ratio of daytime total sensible heat flux to daytime total net radiation (Hs/Rn) was higher than 0.1, the correlation coefficient between the extra resistance and geometric parameters and local climate parameters was 0.63, and the RMSE was 19.78 s/m. When the ratio of sensible heat flux to net radiation was higher than 0.2, the correlation coefficient (r) between r_r and geometric parameters and solar parameters was 0.73 and the RMSE was 14.3 s/m, while the r_r to estimate sensible heat flux could reach more than 100 s/m. When the ratio of sensible heat flux to net radiation was higher, the extra resistance was more sensitive to geometry and solar parameters. In the daytime, the ratio of sensible heat flux to net radiation was generally larger than 0.2 [47]. In other words, in most cases, it was not really necessary to estimate Hs/Rn to determine the appropriate values of the coefficients in Equation (7). Additional comments on this aspect can be found in the discussion in Section 4. Thus, r_r could be parameterized using urban geometric parameters and solar irradiance in the daytime.

Table 3. Parameterization of r_r under different conditions.

Hs/Rn	a_1	a_2	a_3	a_4	a_5	a_6	a_7	*R*	RMSE (s/m)
>0.1	8.32	40.60	−0.056	−0.30	0.001	−5.99	54.56	0.63	19.78
>0.2	7.64	37.30	−0.033	−0.25	0.013	−4.81	36.02	0.73	14.3
>0.3	6.18	31.45	−0.019	−0.074	0.025	−3.99	14.82	0.77	10.16
>0.4	5.52	25.34	−0.017	−0.007	0.026	−3.34	8.63	0.77	8.3

3.3. Evaluation of the Parameterization of r_r

The parameterizations of r_r (Table 3) when H/Rn was larger than 0.2 were evaluated using numerical experiments on 27 February 2010, 1 July 2010, 17 September 2010, and 17 November 2010 (Figure 6). The results show that r_r was underestimated when r_r was larger than 40 s/m. On 27 November, r_r was relatively low since the wind speed was higher than on other days.

The radiometric temperature is much higher than the complete urban surface temperature within urban spaces in the daytime. The main observation targets in an urban canopy are urban roofs and streets at nadir or near-nadir. This overestimates the sensible heat flux when the radiometric temperature is directly used to replace the complete surface temperature to estimate sensible heat flux. Extra resistance r_r should be added when the radiometric temperature over an urban canopy is used for sensible heat flux estimation. Another option is to develop a parameterization scheme of aerodynamic resistance when the radiometric temperature from remote sensing data is used. However, the development of a relation for aerodynamic resistance in sensible heat estimation from the radiometric surface temperature based on urban geometry and climate variables is more complex than adding extra resistance.

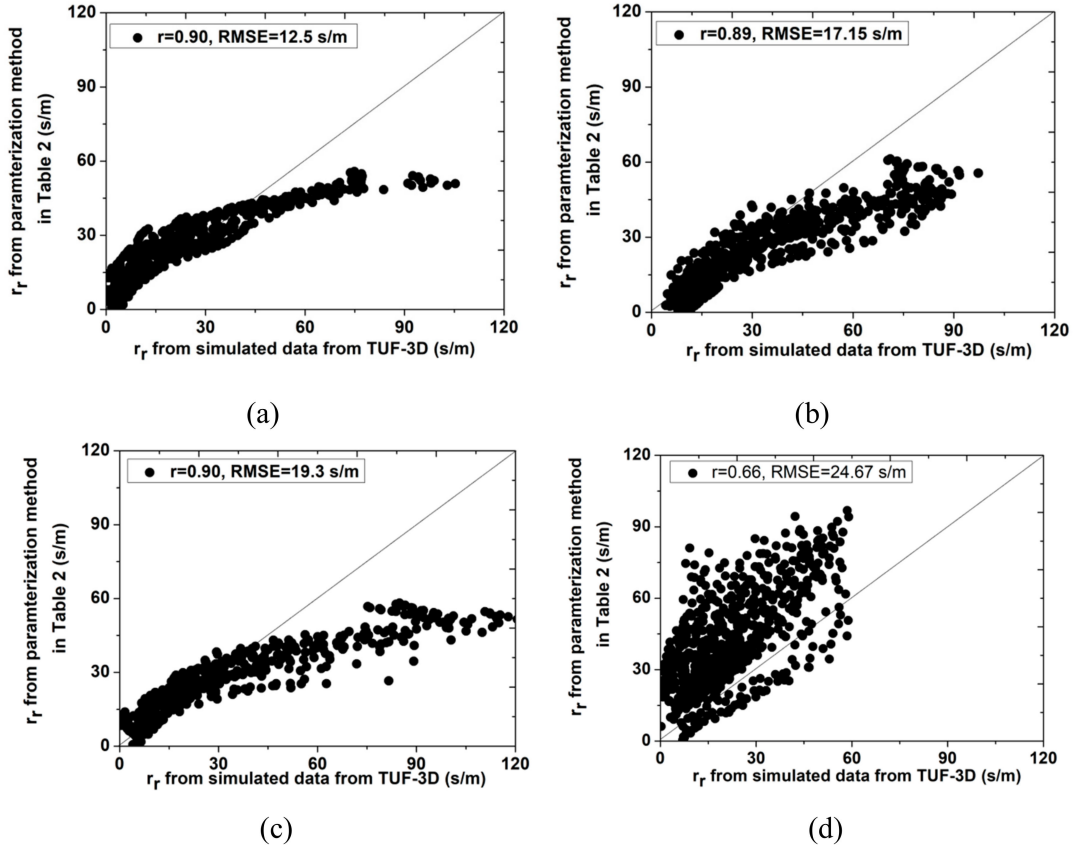

Figure 6. Evaluation of the parameterizations of r_r based on numerical experiments: (**a**) 27 February 2010; (**b**) 1 July 2010; (**c**) 17 September 2010; (**d**) 27 November 2010.

Figure 7 is a comparison of sensible heat fluxes calculated from Equations (2) and (3) and radiometric temperature without considering extra resistance (based on thermal airborne data). The results show that the r^2 and RMSD between the sensible heat flux calculated from the radiometric temperature without r_r and the sensible heat flux from Equation (2) were 0.69 and 147.56 W m^{-2}. The sensible heat flux calculated from radiometric temperature without r_r was much higher than the sensible heat flux from Equation (2). This was because the radiometric temperature observed over an urban canopy is much higher than the complete urban surface temperature within urban spaces. In this study, most roof temperatures were >47 °C, while most wall temperatures were about 31 to 33 °C. Thus, the complete urban surface temperature within the urban area was much lower than the radiometric temperature observed over the urban canopy. Thus, the sensible heat fluxes were overestimated when the radiometric temperature was directly used to estimate the sensible heat flux.

After adding the extra resistance r_r (Equation (3)), the sensible heat flux calculated from radiometric temperature based on Equation (3) was smaller than the sensible heat flux from radiometric temperature without r_r. The results show that the differences in sensible heat fluxes from Equations (2) and (3) were much smaller than the differences in sensible heat fluxes calculated from radiometric temperature without r_r and the sensible heat fluxes from Equation (2). The r^2 and RMSD between the sensible heat fluxes calculated from Equation (2) and the sensible heat fluxes from Equation (3) were 0.79 and 47.98 W m^{-2}. This RMSD was comparable to the accuracy of the eddy covariance (e.g., 50 W m^{-2}), which is an acceptable accuracy for sensible heat flux. Overall, the sensible heat fluxes from Equations (2) and (3) were much closer to each other than the sensible heat fluxes from Equation (2) and the sensible heat fluxes calculated from radiometric temperature without r_r. This suggested that the parameterization of r_r in estimating sensible heat flux using observations of the radiometric temperature was acceptable.

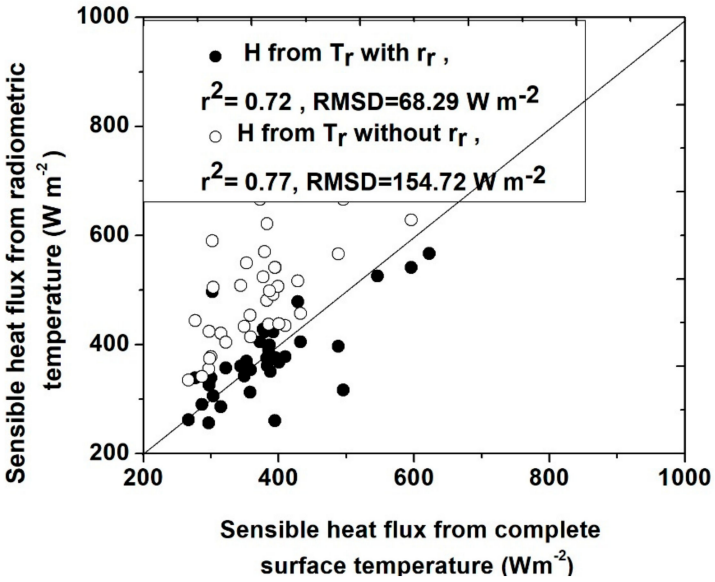

Figure 7. Sensible heat flux estimated by Equations (2) and (3).

4. Discussion

Urban sensible heat flux is an important indicator of urban climate, since it represents the dissipation of excess heat in urban areas. Sensible heat flux estimation from remote sensing data has the ability to provide regional- or large-scale information [12,22,37]. However, whether the bulk transfer method of sensible heat flux estimation applies to radiometric temperature as observed by remote sensing is still not clear. Voogt and Grimmond [11] analyzed the effects of using different surface temperature definitions on the estimation of sensible heat flux based on resistance parameterization methods. Their results showed that surface temperature must be carefully selected for urban sensible heat flux estimation. Kanda et al. [13] analyzed the impact of different representative temperatures (complete surface temperature and radiative temperature) on the estimation of sensible heat flux and estimated the resistances based on different temperatures. Their results showed that there is an obvious difference between the resistances estimated from radiometric temperature and complete surface temperature. The results also showed that there is a seasonal change in roughness length and resistance, while the results did not suggest a significant correlation between solar elevation and the estimated roughness length. This is similar to the results in this study. The solar angle had no obvious effect on the resistance derived from the complete surface temperature, according to our study.

Here, we parameterized resistance for urban sensible heat flux estimations based on nadir radiometric temperatures observed from remote sensing. The results showed that adding extra resistance was a feasible approach. The extra resistance could be parameterized using urban parameters (e.g., a planar area index, wall facet area index) and meteorological variables (e.g., wind speed, solar radiation). Parameterization of the extra resistance was affected by the ratio of sensible heat flux to net radiation, and when the ratio of sensible heat flux to net radiation was lower than 0.1, the parameterization of extra resistance had a larger RMSE compared to a higher ratio of sensible heat flux to net radiation. In our view, the impact of Hs/Rn on the accuracy of the estimated r_r represented an important caveat only when $Hs/Rn < 0.1$. This case is likely to apply when latent heat flux is large, e.g., in urban neighborhoods characterized by a large fraction of vegetation. Under these conditions, additional resistance would still be needed to estimate Hs from T_r, but such resistance would depend on vegetation rather than urban geometry. In the daytime, the ratio of sensible heat flux to net radiation is generally higher than 0.2 [47], and thus the parameterization method for extra resistance could be applied to estimate the urban sensible heat flux and reduce the RMSE when we directly used the radiometric surface temperature.

There were several limitations to this study. There were additional factors that led to errors in sensible heat flux estimation. One factor was that r_r was underestimated when r_r was larger than 40 s/m (Figure 6). Additionally, although the sensible heat flux simulated by TUF-3D has been validated by several measurements [40,43], TUF-3D has several limitations when applied to studies of sensible heat flux. For example, it only deals with uniform building footprints and represents the momentum forcing and associated impacts of turbulence on sensible heat transfer in a simplified fashion. In real urban areas, building shapes and structures are complex and variable, which affects wind flow. Additionally, the wind profile in TUF-3D is parameterized as an exponential canopy wind speed profile. Thus, resistance parameterizations for sensible heat flux based on remote sensing data over urban areas still need more exploration based on field experiment data.

In this study, the parameterization method for extra resistance was only studied for uniform built-up areas. Variations in vegetation and building shape were not considered. For mixed areas with vegetation and buildings, extra resistance for radiometric temperature can be estimated by combining the parameterization methods developed in this study for building areas with the methods for vegetation canopy explored by Reference [36]. Vegetation also affects the distribution of urban surface temperature, and this further affects the difference between radiometric temperature and complete surface temperature. Thus, a combination of the parameterization methods developed in this study for building areas with the methods for vegetation canopy explored by Reference [36] still needs to be explored. When the satellite observation direction changes, the radiometric temperature may change. Thus, directional (non-nadir) radiometric temperature (for estimations of urban sensible heat flux) still needs more exploration. Urban material properties also affect thermal heterogeneity, which affects the difference between complete surface temperature and radiometric temperature. In addition, thermal heterogeneity also affects heat transfers within urban areas [5]. Thus, the estimation of urban sensible heat flux from remote sensing data requires much more exploration.

5. Summary and Conclusions

The estimation of urban sensible heat flux is important for urban climate studies and for assessments of surface–atmosphere convective heat transfer. Direct predictions of urban sensible heat flux based on thermal remote sensing are still limited because of complications related to urban geometry. Radiometric surface temperatures observed from remote sensing platforms cannot capture the corresponding complete urban surface temperature directly, but instead always capture a biased surface temperature that depends on the view direction. This study explored the utility of "effective" resistances for sensible heat flux estimation, enabling the prediction of sensible heat flux from directional (nadir) radiometric surface temperature despite the fact that the complete surface ultimately contributes to total urban sensible heat flux. The results showed that the effective resistance required to assess sensible heat flux from radiometric surface temperature over urban canopies was higher than the resistance required when assessing sensible heat flux from complete urban surface temperature during daytime. Thus, the use of radiometric (i.e., directional, nadir) temperature instead of the complete surface temperature required the addition of extra resistance to prevent large overestimations of sensible heat flux during daytime. The magnitude of this extra resistance was affected by urban geometry and climate conditions, e.g., building or roof plan area, solar radiation, and wind speed, since these parameters affect three-dimensional surface temperature heterogeneity and therefore the difference between the radiometric temperature observed from remote sensing data and the complete urban surface temperature. This study explored different surface temperature definitions and associated resistances for estimations of urban sensible heat fluxes, and the results indicated that an appropriately modified resistance parameterization should be adopted when different temperature definitions are used, and that these parameterizations should be based on local meteorological and urban surface structure conditions.

Author Contributions: J.Y., M.M., and E.S.K., jointly conceived of and designed this study. Z.W. provided suggestions on the experiments. J.Y. processed and analyzed the data and wrote up a draft of the manuscript.

Q.S. and X.O. contributed to editing the different versions of the manuscript and also drawing the figures in the manuscript. All authors made contribution to editing and reviewing this manuscript.

Funding: This work was funded by the National Natural Science Foundation of China under Grant 41671430, Guangzhou University under Grant Number 2900603999, and the National Natural Science Foundation of China under Grant 41571366 and Grant 61601522. Massimo Menenti acknowledges the support of the SAFEA Long-Term-Project of the 1000 Talent Plan for High-Level Foreign Experts (grant no. WQ20141100224).

Acknowledgments: We would like to thank Man Sing Wong for providing the high-resolution data and PW Chan for the meteorological data used in this study.

Conflicts of Interest: The authors declare no conflict of interest.

Appendix A

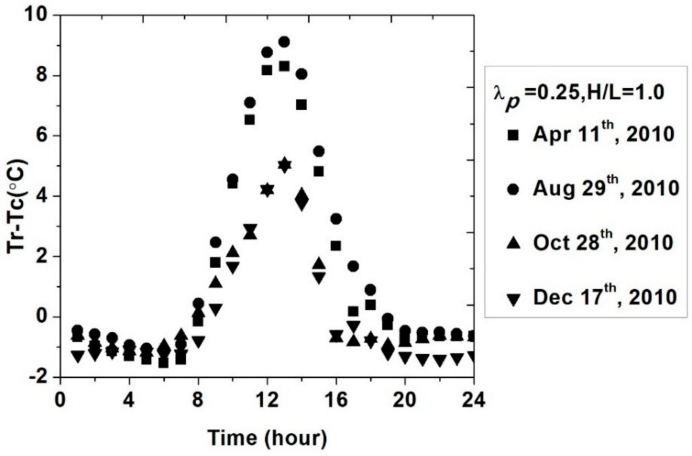

Figure A1. Diurnal plots of the difference between *Tc* and *Tr*.

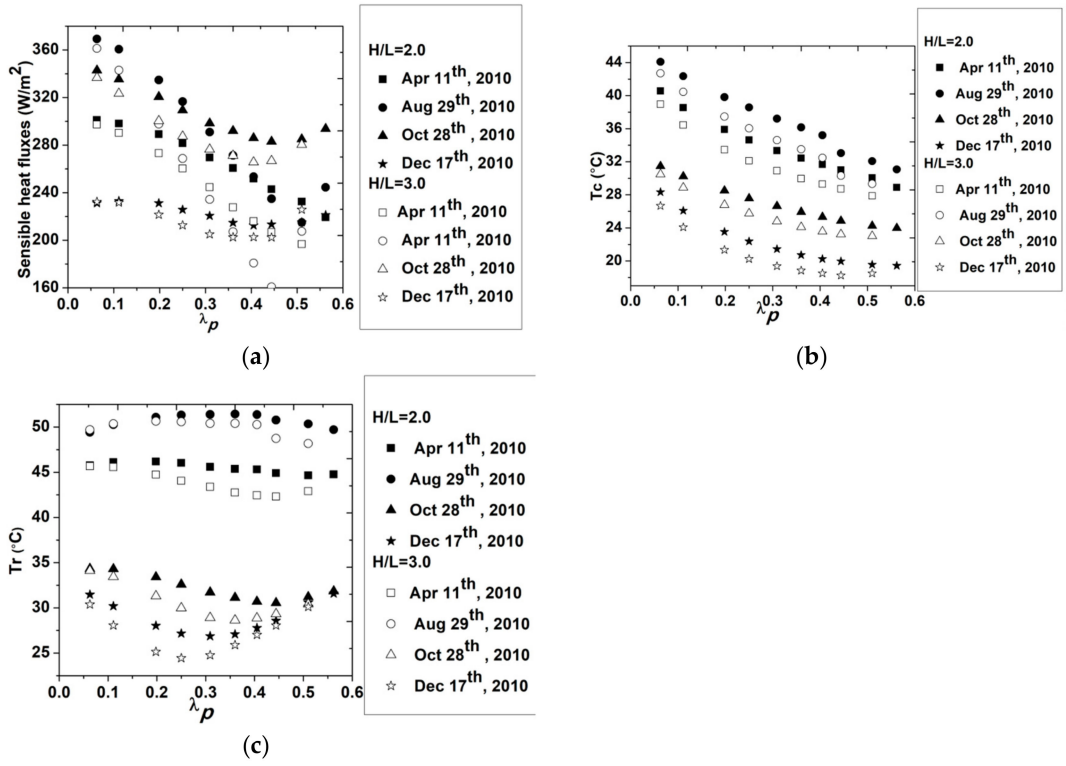

Figure A2. Changes in sensible heat flux (**a**) T_c (**b**) and T_r (**c**) with λ_p.

Table A1. Regressions between resistances and λ_p.

	11 April 2010	29 August 2010	28 October 2010	17 December 2010
$H/L = 2$	$r_h = -78.00 * \lambda_p + 58.68$, $r = 0.99$	$r_h = -75.27 * \lambda_p + 47.16$, $r = 0.98$	$r_h = -47.93 * \lambda_p + 42.17$, $r = 0.99$	$r_h = -84.10 * \lambda_p + 73.53$, $r = 0.95$
	$r_r = 121.02 * \lambda_p + 16.179$, $r = 0.99$	$r_r = 163.89 * \lambda_p + 7.2$, $r = 0.97$	$r_r = 37.35 * \lambda_p + 9.48$, $r = 0.97$	$r_r = 99.54 * \lambda_p + 6.11$, $r = 0.96$
$H/L = 3$	$r_h = -86.01 * \lambda_p + 52.67$, $r = 0.98$	$r_h = -100.17 * \lambda_p + 46.05$, $r = 0.97$	$r_h = -56.39 * \lambda_p + 39.28$, $r = 0.99$	$r_h = -101.49 * \lambda_p + 67.47$, $r = 0.99$
	$r_r = 132.86 * \lambda_p + 20.86$, $r = 0.99$	$r_r = 237.41 * \lambda_p + 7.72$, $r = 0.95$	$r_r = 36.11 * \lambda_p + 10.49$, $r = 0.92$	$r_r = 110.68 * \lambda_p + 5.40$, $r = 0.94$

Table A2. Regressions between resistances and F.

	11 April 2010	29 August 2010	28 October 2010	17 December 2010
$\lambda_p = 0.25$	$r_h = -19.45 * ln\ F + 49.39$, $r = 0.99$	$r_h = -14.2 * ln\ F + 37.13$, $r = 0.99$	$r_h = -12.27 * ln\ F + 36.96$, $r = 0.99$	$r_h = -24.37 * ln\ F + 64.90$, $r = 0.99$
	$r_r = 17.02 * ln\ F + 35.04$, $r = 0.99$	$r_r = 39.79 * ln\ F + 32.40$, $r = 0.92$	$r_r = 4.25 * ln\ F + 15.71$, $r = 0.88$(aspect ratio < 3)	$r_r = 2.14 * ln\ F + 23.86$, $r = 0.67$
$\lambda_p = 0.36$	$r_h = -20.83 * ln\ F + 51.31$, $r = 0.99$	$r_h = -17.48 * ln\ F + 37.13$, $r = 0.99$	$r_h = -14.09 * ln\ F + 38.67$, $r = 0.99$	$r_h = -23.68 * ln\ F + 66.20$, $r = 0.99$
	$r_r = 24.57 * ln\ F + 35.59$, $r = 0.96$	$r_r = 52.36 * ln\ F + 29.56$, $r = 0.94$	$r_r = 2.62 * ln\ F + 18.06$, $r = 0.85$	$r_r = 11.74 * ln\ F + 27.88$, $r = 0.98$

References

1. Oke, T.; Cleugh, H.; Grimmond, C.; Schmid, H.; Roth, M. Evaluation of spatially-averaged fluxes of heat, mass and momentum in the urban boundary layer. *Weather Clim.* **1989**, *9*, 14–21. [CrossRef]
2. Shahmohamadi, P.; Che-Ani, A.I.; Ramly, A.; Maulud, K.N.A.; Mohd-Nor, M.F.I. Reducing urban heat island effects: A systematic review to achieve energy consumption balance. *Int. J. Phys. Sci.* **2010**, *5*, 626–636.
3. Kuang, W.; Dou, Y.; Zhang, C.; Chi, W.; Liu, A.; Liu, Y.; Liu, J. Quantifying the heat flux regulation of metropolitan land use/land cover components by coupling remote sensing modeling with in situ measurement. *J. Geophys. Res. Atmos.* **2015**, *120*, 113–130. [CrossRef]
4. Oke, T.R. The energetic basis of the urban heat island. *Q. J. R. Meteorol. Soc.* **1982**, *108*, 1–24. [CrossRef]
5. Nazarian, N.; Kleissl, J. CFD simulation of an idealized urban environment: Thermal effects of geometrical characteristics and surface materials. *Urban Clim.* **2015**, *12*, 141–159. [CrossRef]
6. Krayenhoff, E.S.; Santiago, J.L.; Martilli, A.; Christen, A.; Oke, T.R. Parametrization of Drag and Turbulence for Urban Neighbourhoods with Trees. *Bound. Layer Meteorol.* **2015**, 1–33. [CrossRef]
7. Nazarian, N.; Martilli, A.; Norford, L.; Kleissl, J. Impacts of Realistic Urban Heating. Part II: Air Quality and City Breathability. *Bound. Layer Meteorol.* **2018**. [CrossRef]
8. Masson, V. A physically-based scheme for the urban energy budget in atmospheric models. *Bound. Layer Meteorol.* **2000**, *94*, 357–397. [CrossRef]
9. Kusaka, H.; Kondo, H.; Kikegawa, Y.; Kimura, F. A simple single-layer urban canopy model for atmospheric models: Comparison with multi-layer and slab models. *Bound. Layer Meteorol.* **2001**, *101*, 329–358. [CrossRef]
10. Martilli, A.; Clappier, A.; Rotach, M. An Urban Surface Exchange Parameterisation for Mesoscale Models. *Bound. Layer Meteorol.* **2002**, *104*, 261–304. [CrossRef]
11. Voogt, J.A.; Grimmond, C. Modeling surface sensible heat flux using surface radiative temperatures in a simple urban area. *J. Appl. Meteorol.* **2000**, *39*, 1679–1699. [CrossRef]
12. Xu, W.; Wooster, M.; Grimmond, C. Modelling of urban sensible heat flux at multiple spatial scales: A demonstration using airborne hyperspectral imagery of Shanghai and a temperature–emissivity separation approach. *Remote Sens. Environ.* **2008**, *112*, 3493–3510. [CrossRef]
13. Kanda, M.; Kanega, M.; Kawai, T.; Moriwaki, R.; Sugawara, H. Roughness lengths for momentum and heat derived from outdoor urban scale models. *J. Appl. Meteorol. Climatol.* **2007**, *46*, 1067–1079. [CrossRef]
14. Kastendeuch, P.P.; Najjar, G. Simulation and validation of radiative transfers in urbanised areas. *Sol. Energy* **2009**, *83*, 333–341. [CrossRef]

15. Krayenhoff, E.S. A Multi-Layer Urban Canopy Model for Neighbourhoods with Trees. Ph.D. Thesis, University of British Columbia, Vancouver, BC, Canada, 2014.
16. Nazarian, N.; Martilli, A.; Kleissl, J. Impacts of Realistic Urban Heating, Part I: Spatial Variability of Mean Flow, Turbulent Exchange and Pollutant Dispersion. *Bound. Layer Meteorol.* **2018**, *166*, 367–393. [CrossRef]
17. Stewart, J.B.; Kustas, W.P.; Humes, K.S.; Nichols, W.D.; Moran, M.S.; De Bruin, H. Sensible heat flux-radiometric surface temperature relationship for eight semiarid areas. *J. Appl. Meteorol.* **1994**, *33*, 1110–1117. [CrossRef]
18. Wang, L.; Li, D.; Gao, Z.; Sun, T.; Guo, X.; Bou-Zeid, E. Turbulent Transport of Momentum and Scalars Above an Urban Canopy. *Bound. Layer Meteorol.* **2014**, *150*, 485–511. [CrossRef]
19. Kanda, M.; Moriwaki, R.; Kasamatsu, F. Spatial Variability of Both Turbulent Fluxes and Temperature Profiles in an Urban Roughness Layer. *Bound. Layer Meteorol.* **2006**, *121*, 339–350. [CrossRef]
20. Kato, S.; Yamaguchi, Y. Estimation of storage heat flux in an urban area using ASTER data. *Remote Sens. Environ.* **2007**, *110*, 1–17. [CrossRef]
21. Zhou, Y.; Weng, Q.; Gurney, K.R.; Shuai, Y.; Hu, X. Estimation of the relationship between remotely sensed anthropogenic heat discharge and building energy use. *ISPRS J. Photogramm. Remote Sens.* **2012**, *67*, 65–72. [CrossRef]
22. Weng, Q.; Hu, X.; Quattrochi, D.A.; Liu, H. Assessing Intra-Urban Surface Energy Fluxes Using Remotely Sensed ASTER Imagery and Routine Meteorological Data: A Case Study in Indianapolis, USA. *IEEE J. Sel. Top. Appl. Earth Obs. Remote Sens.* **2013**, *7*, 4046–4057. [CrossRef]
23. Wong, M.S.; Yang, J.; Nichol, J.; Weng, Q.; Menenti, M.; Chan, P. Modeling of Anthropogenic Heat Flux Using HJ-1B Chinese Small Satellite Image: A Study of Heterogeneous Urbanized Areas in Hong Kong. *IEEE Geosci. Remote Sens. Lett.* **2015**, *12*, 1466–1470. [CrossRef]
24. Yang, J.; Wong, M.S.; Menenti, M. Effects of Urban Geometry on Turbulent Fluxes: A Remote Sensing Perspective. *IEEE Geosci. Remote Sens. Lett.* **2016**, *13*, 1767–1771. [CrossRef]
25. Marconcini, M.; Heldens, W.; Del Frate, F.; Latini, D.; Mitraka, Z.; Lindberg, F. EO-based products in support of urban heat fluxes estimation. In Proceedings of the 2017 Joint Urban Remote Sensing Event (JURSE), Dubai, United Arab Emirates, 6–8 March 2017; pp. 1–4.
26. Zheng, Y.; Weng, Q. Evaluation of the correlation between remotely sensing-based and GIS-based anthropogenic heat discharge in Los Angeles County, USA. In Proceedings of the 2016 4th International Workshop on Earth Observation and Remote Sensing Applications (EORSA), Guangzhou, China, 4–6 July 2016; pp. 324–328.
27. Chrysoulakis, N.; Heldens, W.; Gastellu-Etchegorry, J.-P.; Grimmond, S.; Feigenwinter, C.; Lindberg, F.; Del Frate, F.; Klostermann, J.; Mitraka, Z.; Esch, T. A novel approach for anthropogenic heat flux estimation from space. In Proceedings of the 2016 IEEE International Geoscience and Remote Sensing Symposium (IGARSS), Beijing, China, 10–15 July 2016; pp. 6774–6777.
28. Luo, H.; Liu, C.; Wu, C.; Guo, X. Urban Change Detection Based on Dempster–Shafer Theory for Multitemporal Very High-Resolution Imagery. *Remote Sens.* **2018**, *10*, 980. [CrossRef]
29. Ouyang, X.; Chen, D.; Duan, S.-B.; Lei, Y.; Dou, Y.; Hu, G. Validation and Analysis of Long-Term AATSR Land Surface Temperature Product in the Heihe River Basin, China. *Remote Sens.* **2017**, *9*, 152. [CrossRef]
30. Su, Z. The Surface Energy Balance System (SEBS) for estimation of turbulent heat fluxes. *Hydrol. Earth Syst. Sci.* **1999**, *6*, 85–100. [CrossRef]
31. Voogt, J.A.; Oke, T.R. Complete urban surface temperatures. *J. Appl. Meteorol.* **1997**, *36*, 1117–1132. [CrossRef]
32. Jiang, L.; Zhan, W.; Voogt, J.; Zhao, L.; Gao, L.; Huang, F.; Cai, Z.; Ju, W. Remote estimation of complete urban surface temperature using only directional radiometric temperatures. *Build. Environ.* **2018**, *135*, 224–236. [CrossRef]
33. Yang, J.; Wong, M.S.; Menenti, M.; Nichol, J.; Voogt, J.; Krayenhoff, E.S.; Chan, P.W. Development of an improved urban emissivity model based on sky view factor for retrieving effective emissivity and surface temperature over urban areas. *ISPRS J. Photogramm. Remote Sens.* **2016**, *122*, 30–40. [CrossRef]
34. Shi, Q.; Liu, X.; Huang, X. An Active Relearning Framework for Remote Sensing Image Classification. *IEEE Trans. Geosci. Remote Sens.* **2018**, *56*, 3468–3486.
35. Troufleau, D.; Lhomme, J.P.; Monteny, B.; Vidal, A. Sensible heat flux and radiometric surface temperature over sparse Sahelian vegetation. I. An experimental analysis of the kB−1 parameter. *J. Hydrol.* **1997**, *188*, 815–838. [CrossRef]

36. Zhao, L.; Lee, X.; Suyker, A.; Wen, X. Influence of Leaf Area Index on the Radiometric Resistance to Heat Transfer. *Bound. Layer Meteorol.* **2015**, 1–19. [CrossRef]
37. Kato, S.; Yamaguchi, Y. Analysis of urban heat-island effect using ASTER and ETM+ Data: Separation of anthropogenic heat discharge and natural heat radiation from sensible heat flux. *Remote Sens. Environ.* **2005**, *99*, 44–54. [CrossRef]
38. Liu, Y.; Shintaro, G.; Zhuang, D.; Kuang, W. Urban surface heat fluxes infrared remote sensing inversion and their relationship with land use types. *J. Geogr. Sci.* **2012**, *22*, 699–715. [CrossRef]
39. Grimmond, C.; Oke, T.R. Aerodynamic properties of urban areas derived from analysis of surface form. *J. Appl. Meteorol.* **1999**, *38*, 1262–1292. [CrossRef]
40. Krayenhoff, E.S.; Voogt, J. A microscale three-dimensional urban energy balance model for studying surface temperatures. *Bound. Layer Meteorol.* **2007**, *123*, 433–461. [CrossRef]
41. Krayenhoff, E.S.; Christen, A.; Martilli, A.; Oke, T.R. A Multi-layer Radiation Model for Urban Neighbourhoods with Trees. *Bound. Layer Meteorol.* **2014**, *151*, 139–178. [CrossRef]
42. Krayenhoff, E.S.; Voogt, J.A. Daytime Thermal Anisotropy of Urban Neighbourhoods: Morphological Causation. *Remote Sens.* **2016**, *8*, 108. [CrossRef]
43. Crawford, B.; Krayenhoff, E.S.; Cordy, P. The urban energy balance of a lightweight low-rise neighborhood in Andacollo, Chile. *Theor. Appl. Climatol.* **2016**, 1–14. [CrossRef]
44. Becker, F.; Li, Z.L. Surface temperature and emissivity at various scales: Definition, measurement and related problems. *Remote Sens. Rev.* **1995**, *12*, 225–253. [CrossRef]
45. Stewart, I.D.; Oke, T.R.; Krayenhoff, E.S. Evaluation of the 'local climate zone' scheme using temperature observations and model simulations. *Int. J. Climatol.* **2014**, *34*, 1062–1080. [CrossRef]
46. Nazarian, N.; Fan, J.; Sin, T.; Norford, L.; Kleissl, J. Predicting outdoor thermal comfort in urban environments: A 3D numerical model for standard effective temperature. *Urban Clim.* **2017**, *20*, 251–267. [CrossRef]
47. Grimmond, C.; Oke, T.R. Turbulent heat fluxes in urban areas: Observations and a local-scale urban meteorological parameterization scheme (LUMPS). *J. Appl. Meteorol.* **2002**, *41*, 792–810. [CrossRef]